Front. Struct. Civ. Eng. 2025, 19(1): 60–75
https://doi.org/10.1007/s11709-025-1156-9

RESEARCH ARTICLE

An Elman neural network approach in active control for building vibration under earthquake excitation

Xuan-Thuan NGUYEN, Hong-Hai HOANG, Hai-Le BUI*, Thi-Thoa MAC

School of Mechanical Engineering, Hanoi University of Science and Technology, Hanoi 100000, Vietnam
**Corresponding author. E-mail: le.buihai@hust.edu.vn*

ABSTRACT This article presents an improved Elman neural network for reducing building vibrations during earthquakes. The adjustment coefficient is proposed to be added to the Elman network's output layer to improve the controller's performance when used to minimize vibrations in buildings. The parameters of the proposed Elman neural network model are optimized using the Balancing Composite Motion Optimization algorithm. The effectiveness of the proposed method is assessed using a three-story structure with an active dampening mechanism on the first level. The study also takes into account two kinds of Elman neural network input variables: displacement and velocity data on the first floor, as well as displacement and velocity readings across all three floors. This research uses two measures of fitness functions in the optimal process, the structure's peak displacement and acceleration, to determine the best parameters for the proposed model. The effectiveness of the proposed method is demonstrated in restraining the vibration of the structure under a variety of earthquakes. Furthermore, the findings indicate that the proposed model maintains sustainability even when the maximum value of the actuator device is dropped.

KEYWORDS building, vibration, earthquakes, Elman neural network, Balancing Composite Motion Optimization algorithm

1 Introduction

In the process of urbanization, the development and construction of infrastructure and architectural works not only necessitate aesthetic form but also ensure the general safety of these structures against the impact of natural disasters such as storms, tornadoes, earthquakes, etc. Strong earthquakes are often devastating, causing serious injuries and extensive property damage. Therefore, in recent decades, numerous research projects have focused on maintaining durability and optimizing the protection of structures during powerful earthquakes. To deal with the high vibration caused by these earthquakes, different types of vibration reduction methods are used to absorb and dissipate the impact energy, such as the passive control [1–3], the semi-active control [4,5], the active control [6–9], and the hybrid control [10] methods. The passive control method is recognized as a method that operates without the need for external energy [11,12]. Instead, these methods employ physics and mechanics principles to absorb and distribute the vibration signal. Since then, the passive control-based system has been able to restrain vibration under different environmental conditions, such as wind, earthquake, and storm. Some typical passive control devices include a Tuned Mass Damper (TMD) [13], Viscous Damper [14], Friction Damper [15], Base Isolator [16], Viscoelastic Damper [17], and so on. Li and Zhang [18] analyzed a type of TMD to mitigate the vibration of a linear primary structural subject to harmonic excitation. Sharma et al. [19] analyzed the efficiency of the fluid viscous dampers in restraining the structural vibrations under earthquake excitation. Barzegar et al. [20] presented a friction damper for reducing earthquake-induced vibrations. Li et al. [21] developed a system to restrain the vibration of a multi-degree-of-freedom structure using a TMD. Zhou et al. [22] proposed a response-based seismic design for a structure device based on viscoelastic dampers. Although passive control methods have some benefits to some extent, they also contain some inherent disadvantages.

Article history: Received Jul 3, 2024; Accepted Sep 15, 2024

These control systems are often designed to operate most effectively at a specific vibration frequency. As a result, sudden changes in the vibration frequency of the building structure due to unexpected environmental factors can significantly reduce control effectiveness. In addition, passive control systems have a limited ability to absorb vibration energy compared to other kinds of control systems, so they may not be enough to protect buildings during powerful earthquakes. Moreover, due to their lack of self-adjusting ability, passive control systems often respond slowly in emergencies. The semi-active control method is defined as a method that could calibrate the mechanic attributes in real-time [23–26]. Unlike the passive control method, the semi-active control method requires a portion of external energy to calibrate the parameters on the vibration device. This makes the semi-active control method more adaptable within a certain range than the traditional method. In other words, based on the flexible adjustment capability, the semi-active control methods can reduce vibrations more effectively than the passive control methods, especially under sudden external forces. Some typical passive control methodologies include Magnetorheological (MR) Damper [27], Electrorheological (ER) Damper [28], and so on. Bhowmik and Debnath performed the MR damper using Linear Quadratic Regulator (LQR) control for building protection under seismic events [29]. Tang et al. [30] used a fuzzy controller with an ER damper for seat suspension vibration. Even though semi-active controllers often release quick responses compared to passive control methods, they still have some time delays during the parameter calibration process. As a result, the overall accuracy of vibration reduction may be compromised. Additionally, the semi-active controllers could only change some mechanic attributes of the vibration reduction device, such as stiffness and damper. They cannot themselves create the control force and they are limited in the ability of the vibration control in some cases. The active control method is known as a method that could create the control force directly against the vibration phenomena [10,31–33]. These methodologies use the measured data from the sensor system to calculate the structure's response signal. After that, these values are applied as the inputs of the controller system for generating the suitable force to restrain the vibration. Some typical passive control methodologies include Active Mass Dampers [34], Active Tendon Systems [35], Active Bracing Systems [36]. Active control methods offer several advantages over other types of controllers. First, the active control methods can adjust system parameters in real-time based on changing operating conditions and environmental factors. This helps ensure the optimal performance of the designed system in a continuous way. Secondly, they can respond rapidly to disturbances and sudden changes, maintaining system stability and efficiency.

Nowadays, artificial intelligence (AI) has permeated nearly every sector of human life, offering innovative solutions and efficiencies that were once thought impossible for many scientific fields. At its core, AI involves the creation of systems capable of performing tasks that typically require human intelligence. These tasks range from daily normal actions [37–39] to complex processes [40–42]. With breakthrough developments in the 4.0 era, AI extends significant impact and efficiency to support solving some of humanity's most pressing challenges, such as natural disaster prediction and infrastructure protection. In recent years, some studies have been conducted on using AI neural networks to predict vibration and damage to structures under the influence of different environmental factors [43–49]. Zizouni et al. [50] presented a neural network controller to protect the structure under seismic excitation. The effectiveness of the method is confirmed by the reduction of the structure in two cases of earthquakes. However, this research has not yet considered the parameters of the neural network. Consequently, the method did not achieve its maximum effectiveness. Goswami et al. [51] suggested a new approach to deal with brittle fracture problems by aiding a physics-informed neural network (PINN). The proposed approach concentrated on imposing boundary conditions to minimize the variational energy of the system. In addition, the transfer learning method was also used for partial retraining of the network while keeping certain weights and biases fixed. This allowed for a more effective resolution of potential training inefficiencies. However, the paper still has some minor issues related to the residual-based formulation and the inability to capture sharp discontinuities in the system. This limitation could hinder the proposed approach's performance in scenarios where such discontinuities are significant.

Qiu and Wang [52] proposed a fuzzy neural network (FNN) with five layers to suppress the vibration of a piezoelectric flexible hinged plate. The experimental results showed the usefulness of the method in comparison with proportional-derivative controllers. However, the article had not yet investigated the system's case under random dynamic loading. Paneiro and Rafael [53] investigated forecasting ground vibration amplitude induced by subsurface explosions using a neural network technique. This paper employed the bilevel optimization approach to enhance the neural network design. By determining the ideal number of neurons for the hidden layer, the optimization strategy improves the performance of the neural network. If the hidden layer of the neural network has more processing units, it may be able to learn and predict the magnitude of ground vibrations more precisely. One limitation is that the proposed neural network technique focuses only on blast-induced ground vibration predictions, which may limit its use outside of

instrumental applications such as earthquake or wind vibration. Li et al. [54] proposed a controller method based on adaptive neural networks for vibration reduction in a flexible double-clamped beam system. However, the paper does not consider changing the external disturbance in the beam system to demonstrate the effectiveness of the control method, nor does it investigate the impact on the efficiency of changing the neural network parameters. Yan et al. [55] used an Active TMD together with a FNN approach. The FNN method enhanced the control process by allowing intelligent decision-making using fuzzy logic and neural network theory. The study's limitation was that it did not consider the importance of the control force. This might affect the control method's robustness. Brancati et al. [56] proposed employing a semi-active technology to dampen vibrations in lightweight structures. To improve the controller, they advocated merging a neural network with a model predictive control approach. However, this technique was only tested on a model during the El Centro earthquake and might not be applicable to other earthquakes. Yucesan et al. [57] presented a PINN framework to adjust the control signals for the torsional vibration damper. By combining physics-based models and a neural network-based data-driven approach, the proposed framework updated the parameters of the torsional vibration damper using experimental data. However, since this framework used the Kennedy and O'Hagan approach, which mostly relies on Gaussian process modeling, the input variables of the proposed model were not along in a large-scale range. Xing and Liu [58] developed a control system using neural adaptive techniques to reduce vibration for the three-dimensional Timoshenko beam. To be more detailed, the nonlinear dynamic mechanism of the structure model was first defined by applying the partial differential equations. Based on that, the output restrictions of the control system were restricted by using the barrier Lyapunov functions and the neural adaptive control scheme. Finally, the performance of the proposed controller system was evaluated via numerical simulations. However, the research did not investigate the effects of sensor placement, sampling rates, and noise chattering on the control system. Zhang et al. [59] introduced a combined method for reducing irregular wave-induced vibrations on offshore platforms. This method was established by combining neural networks and fuzzy logic to create an efficient controller that adapts to random time delays and restrains vibration phenomena. Nevertheless, the proposed model has not considered the appearance of disturbance forces during offshore operations or optimized the neural network's parameters. Zhang et al. [60] proposed an elevator horizontal vibration control rule for MR damper devices based on the firefly algorithm and FNNs' backpropagation technique. The study's limitation was that it did not evaluate the efficacy of the elevator vibration research technique under various external loads. Furthermore, the optimization technique only applies to a specific system situation. As a result, the controller may not be sufficiently generic to be useful in reality. Yu et al. [61] proposed a real-time control strategy for reducing structural vibrations using a neural network and a semi-active control approach. By incorporating neural networks into advanced control algorithms, the suggested method could make predictions and decisions based on real-time data to improve the overall vibration control performance. Nevertheless, the control strategy's effectiveness heavily depended on the accuracy and generalization ability of the neural network models. This could lead to the vibration parameters not being optimized, and uncertainties and variations in real-world scenarios could impact the operation ability of the model. Song et al. [62] suggested a controlling model for cantilever structure based on the nonlinear autoregressive with exogenous input (NARX) neural network. By employing the NARX neural network for dynamic model identification, the study could achieve efficient and accurate nonlinear vibration suppression for the cantilever structure in certain cases. Even though the results demonstrated the effectiveness of the proposed model in achieving vibration suppression, it might not address the potential real-time implementation problems that may arise in unpredictable environments. This study also found that adding more input nodes to the NARX neural network could decrease identification error rates but also significantly increase the calculation amount. This showed that there is a trade-off between model accuracy and computational complexity. The authors in Ref. [63] designed a neural network-based sliding mode fuzzy controller for suppressing the flexible beam structure vibration. By using the finite element methodology, the characteristics of the vibration signal were determined. Based on these obtained features, the proposed controller established a robust control process and eliminated the chattering phenomenon. Nonetheless, the proposed controller still had high accumulation errors on the model mechanism caused by the finite element strategy. Gheni et al. proposed an adaptive LQR model for active vibration control [64]. The control signals of the LQR model were adjusted in a larger range and calibrated by utilizing a deep reinforcement learning framework. The results indicated that the proposed model has some improvements in vibration reduction compared to the traditional LQR method. However, this research focuses mainly on simulations with a 3-story building structure and has not examined different types of buildings. In Ref. [65], Zhang and Xue proposed a smart hybrid method to control vibrations in tall buildings. Based on combining the genetic algorithm and the Long Short-term Memory network, the proposed method could construct a structural response prediction and then combine the computation

data with vibration control theory to establish the vibration reduction process. Since the proposed method was based on specific benchmark models and has not yet deeply discussed the complexity involved, it may not accurately reflect all the possible scenarios that tall buildings may encounter in real life. It is obvious that much of the research mentioned concentrated on controlling the vibration under the impact of certain loads. Most of the mentioned controllers have not been tested with multiple types of inputs and could only be applied in some case studies. This could make the control laws too specific and inappropriate under different environmental conditions. In addition, even though the tendency to use an AI neural network to design vibration control methods has broadened and developed, vibration reduction for structures with random dynamic loads such as high-speed wind, storms, or earthquakes is still a major challenge in this field.

It is noteworthy that no research has been used the Elman neural network (ENN) to manage building vibrations during earthquakes. Furthermore, there has been no previous research on developing, building or improving an ENN especially designed to reduce structural vibration caused by seismic activity. This paper presents an improved ENN model that adds an extra adjustment factor for the network output to mitigate earthquake-induced building vibration. The parameters of the improved ENN model are optimized using the Balancing Composite Motion Optimization (BCMO) algorithm to provide the greatest performance and could be used in a variety of earthquakes. The findings reveal that the suggested method has validated the usefulness of the proposed ENN network with optimum parameters in decreasing the fluctuations of various earthquakes, including the El Centro, Kern County, Tabas, Northridge, Kobe, Duzce, and Kocaeli earthquakes. In addition, the robustness of the proposed method is evaluated by examining its efficacy when the maximum control force value is dropped by 80% and 90%, respectively.

The rest of this paper is structured as follows: The next section describes the modeling of the three-floor structure. Section 3 presents the control algorithm based on the ENN model. Section 4 illustrates the optimal algorithm for the designed controller. Section 5 analyzed the numerical results, followed by a brief conclusion in Section 6.

2 Modeling of the three-floor structure

In this research, the model of a three-story building is investigated to evaluate the effectiveness of the proposed controller. The active device is installed on the first floor to restrain the building vibration, as shown in Fig. 1 [66,67].

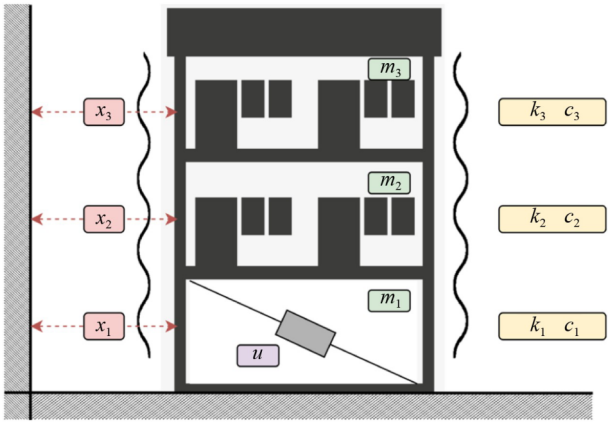

Fig. 1 The structure of the three-story building model.

The vibration equation of the three-story building model is expressed as follows:

$$
\begin{aligned}
&\boldsymbol{M}\ddot{\boldsymbol{x}}+\boldsymbol{C}\dot{\boldsymbol{x}}+\boldsymbol{K}\boldsymbol{x}=-\boldsymbol{M}\times\nabla\times\ddot{x}_{\mathrm{g}}+\boldsymbol{u},\\
&\boldsymbol{x}=[\,x_1 \quad x_2 \quad x_3\,]^{\mathrm{T}},\\
&\dot{\boldsymbol{x}}=[\,\dot{x}_1 \quad \dot{x}_2 \quad \dot{x}_3\,]^{\mathrm{T}},\\
&\boldsymbol{M}=\begin{bmatrix} m_1 & 0 & 0\\ 0 & m_2 & 0\\ 0 & 0 & m_3 \end{bmatrix},\\
&\boldsymbol{C}=\begin{bmatrix} c_1+c_2 & -c_2 & 0\\ -c_2 & c_2+c_3 & -c_3\\ 0 & -c_3 & c_3 \end{bmatrix},\\
&\boldsymbol{K}=\begin{bmatrix} k_1+k_2 & -k_2 & 0\\ -k_2 & k_2+k_3 & -k_3\\ 0 & -k_3 & k_3 \end{bmatrix},\\
&\nabla=[\,-1 \quad 1 \quad 1\,]^{\mathrm{T}},\\
&\boldsymbol{u}=[\,u \quad 0 \quad 0\,]^{\mathrm{T}},
\end{aligned}
\tag{1}
$$

whereas: $\boldsymbol{x}$ represents the displacement vector of the building floors; $\dot{\boldsymbol{x}}$ is the velocity of the building floors; $\ddot{\boldsymbol{x}}$ is the acceleration vector of the building floors; $\boldsymbol{M}$ is the mass matrix of the three-story building model; $\boldsymbol{C}$ is the damping matrix of the building model; $\boldsymbol{K}$ is the stiffness matrix of the building model; ∇ is the vector of earthquake acceleration effect; $\boldsymbol{u}$ denotes the active control force; $\ddot{x}_{\mathrm{g}}$ depicts the acceleration of testing earthquake applied to the building model.

3 Control algorithm based on Elman neural network

Prediction, classification, and control applications make substantial use of the ENN Network, a versatile and evolving artificial neural network technology. Vibration-damping devices use the ENN network to optimize the reduction of damage factors' impact on the system,

resulting in an effective and adaptive solution for program vibration management. ENN networks are made up of three basic components: the input layer, the hidden layer, and the output layer. The input layer is where the network gets its input signals. In the case of dampers, these signals may comprise sensor data such as rate of rise, rate of change, and other system-state parameters. The hidden layer of the Elman network processes and stores temporal information. The Elman network uses context nodes to preserve the previous state of the buried layer. This context node obtains data from the previous cycle's hidden layer and applies it to the current cycle. This enables the network to retain and use prior information, making the Elman network suitable for time series data, especially oscillating data. The hidden layer, together with the context node, contributes to a short memory restriction, allowing the network's capacity to increase over time as anticipated values change. The output layer defines the network's expectations—in this case, the incentive to reduce concussive injury. This output value is used to control the system, eliminate vibrations, and improve overall performance.

This study recommended an additional research upgrade for the ENN system that would improve control quality by adding the adjustment coefficients in the ENN network's output layer. This crucial number not only keeps the network operational but also improves prediction accuracy and force control, lowering operating efficiency. With major changes to the output layer, the proposed network can better respond to the task of changing input data from various earthquake values. This construction reduces vibrations in a range of seismic zones, enabling the system to function more reliably and efficiently. The structure of the improved ENN model and the parameter explanation are depicted in Table 1 and Fig. 2.

As shown in Fig. 2, the improved ENN model contains three different layers in total. First, the input layer imports the initial signals. Next, these signals are transmitted to the neural in the hidden and context layers. Once the calculation is complete, the signals are transported to the output and combined with the critical weights to produce the output results.

To boost the efficiency of the improved ENN model, the following parameters are concentrated for process optimization: the number of neural in the hidden layer, the weights that connect the output layer and the hidden layer, the weights that connect the context layer and the hidden layer, and learning rates. Furthermore, the critical weights, namely "adjustment coefficients," are also proposed to calibrate the values of the output layer.

To simplify the calculation process, the values of the weights connecting the neural of the hidden layer and the neural of the input layer are chosen equally, as shown in Eqs. (2) and (3):

$$w^{\mathrm{h,i}}(t) = w_{ab}^{\mathrm{h,i}}(t),\ \forall a \in \{1,...,m\};\ \forall b \in \{1,...,n\}, \tag{2}$$

$$w^{\mathrm{h,i}}(t) = w^{\mathrm{h,i}}(t-1) - \eta \times \frac{\partial E}{\partial w^{\mathrm{h,i}}(t-1)}. \tag{3}$$

Similarly, the weights between the hidden layers and the context layers $w_{ab}^{\mathrm{h,c}}(t)$and the weights between the output layers and the hidden layers $w_{ab}^{\mathrm{h,c}}(t)$are computed as:

$$w^{\mathrm{h,c}}(t) = w_{ab}^{\mathrm{h,c}}(t),\ \forall a \in \{1,...,m\};\ \forall b \in \{1,...,n\}, \tag{4}$$

$$w^{\mathrm{o,h}}(t) = w_{ab}^{\mathrm{o,h}}(t),\ \forall a \in \{1,...,m\};\ \forall b \in \{1,...,n\}. \tag{5}$$

The parameters of the proposed ENN model are then calculated as follows:

$$h_j = \mathrm{tansig}\left[\left(\sum_{t=1}^{n} x_t \times w^{\mathrm{h,i}}\right) + \left(\sum_{t=1}^{n} c_t \times w^{\mathrm{h,c}}\right)\right];\ \forall j \in \{1,...,m\}, \tag{6}$$

$$y = \mathrm{tansig}\left(\sum_{j=1}^{m} w^{\mathrm{o,h}} \times h_j\right). \tag{7}$$

In this research, the control force for the vibration reduction is computed by multiplying the values of the

Table 1 The parameter explanation of the improved ENN model

Layer	Symbol	Detail
Input layer	$x_1, x_2, ..., x_n$	the input signals
	$w_{ab}^{\mathrm{h,i}},\ \forall a \in \{1,...,m\};\forall b \in \{1,...,n\}$	the weight connects the ath neuron of the hidden layer and the bth neuron of the input layer.
Context layer	$c_1, c_2, ..., c_n$	the neurons of the context layer
	$w_{ab}^{\mathrm{h,c}},\ \forall a \in \{1,...,m\};\forall b \in \{1,...,n\}$	the weight connects the ath neuron of the hidden layer and the bth neuron of the context layer.
Hidden layer	$h_1, h_2, ..., h_m$	the neurons of the hidden layer
Output layer	$y_1, y_2, ..., y_l$	the output results
	$w_{y_1}, w_{y_2}, ..., w_{y_l}$	the proposed critical weights
	$w_{ab}^{\mathrm{o,h}},\ \forall a \in \{1,...,m\};\forall b \in \{1,...,n\}$	the weight connects the ath neuron of the hidden layer and the bth neuron of the output layer.

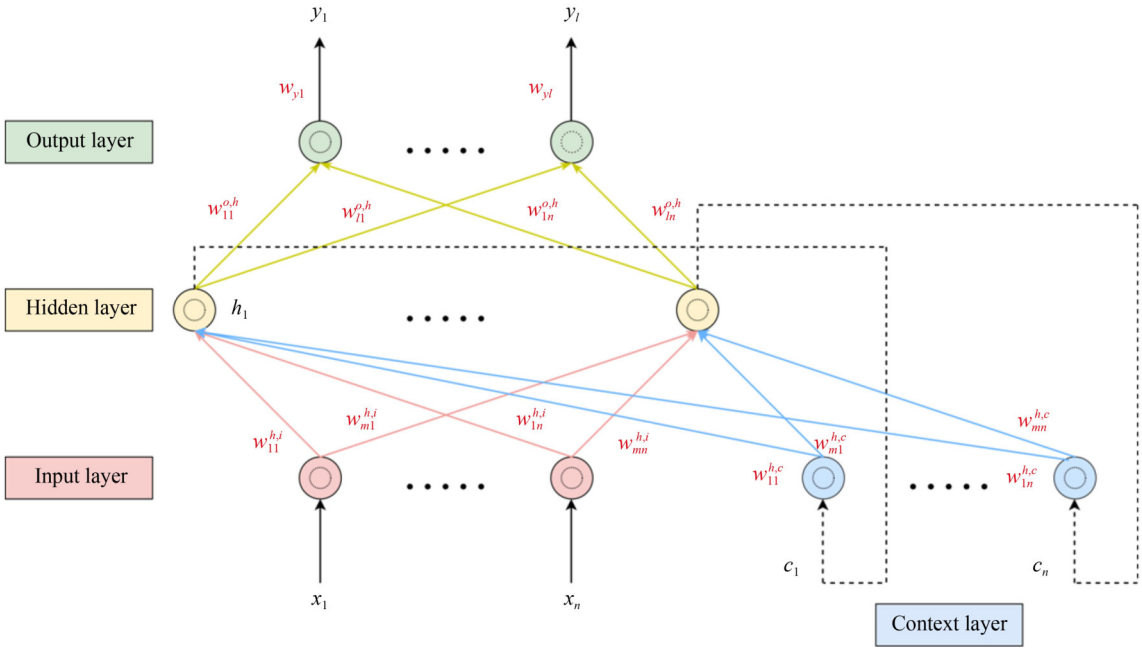

Fig. 2 The general structure of the improved ENN model.

output layers by the proposed adjustment coefficients w_y, as indicated in Eq. (8):

$$u = w_y \times y. \tag{8}$$

4 Optimal algorithm for controller

This research discusses the use of the BCMO algorithm [68] to optimize the core parameters in the Elman neural network to improve its performance. BCMO is a metaheuristic optimization algorithm with many advantages that have been proven in some published studies [69–71]. BCMO is based on the balance between two search strategies.

1) Global Search: Explore the entire search space to find promising regions containing good solutions.

2) Local Search: Searche for better solutions in the neighborhood of existing solutions.

The BCMO algorithm considers the Elman network parameters that need optimization as individual targets.

Step 1. Initialization.

Create an initial population: Each individual represents a set of parameter values for the Elman network. The parameters to be optimized as per the paper include the number of neurons in the hidden layer, weights between the input layer and the hidden layer, weights between the hidden layer and the output layer, weights between the context layer and the hidden layer, learning rates, adjustment coefficients (parameter for fine-tuning the output layer value).

Initialize each parameter value in each individual randomly within a predefined reasonable range.

Determine the global optimal point and the individual.

Calculate the composite motion to determine the position of the individual. The motion vector of the individual ith in each generation with respect to the overall optimal point is denoted as and is calculated by:

$$v_i^g = v_i^{g-1} + \alpha\left(u_i^g - v_i^{g-1}\right) + \beta\left(v_i^g - x_g\right), \tag{9}$$

whereas: v_i^g denotes the displacement of the ith individual in the gth generation. It depicts the individual's movement distance in the search space compared to their initial position. v_i^{g-1} represents the displacement of the ith individual (g–1)th the previous generation. It reflects the individual's position relative to their starting point up to the (g–1)th generation. u_i^g: This term represents the "ideal" movement direction for the ith individual in the gth generation. The u_i^g points toward a promising region of the search space identified by the global search strategy. x_g is the position of the current best solution (individual) found so far in the gth generation. $\alpha \in [0;1]$ is the parameter that controls the influence of the exploration term $\left(u_i^g - v_i^{g-1}\right)$ on the overall movement. $\beta \in [0;1]$ is the weighting factor that controls the influence of the exploitation term $(v_i^g - x_g)$ on the overall movement.

Step 2. Evaluate the performance of each individual in the population: Use the objective function to measure the success of an individual. In this case, two objective functions representing two evaluation criteria of the system, namely displacement and acceleration, are proposed as follows.

$$J_{\mathrm{D}} = \max_{j=1:n}\left(\frac{\max|d_j|}{\max|d_{j,\mathrm{UC}}|}\right) \rightarrow \min, \tag{10}$$

$$J_{\mathrm{D}} = \max_{j=1:n}\left(\frac{\max|d_j|}{\max|d_{j,\mathrm{UC}}|}\right) \rightarrow \min, \tag{11}$$

where d_j and a_j are the relative displacement (RD) and the absolute acceleration (AA) of the jth floor, respectively; $d_{j,\mathrm{UC}}$ and $a_{j,\mathrm{UC}}$ are the RD and the AA of the jth floor of the structure in the case without the controller, respectively.

Step 3. Apply operators to generate new individuals.

Global Search: Employ the mutation operator to alter the values of some parameters in an individual, enabling the exploration of new regions of the search space.

Local Search: Utilize the crossover operator to combine parameters from "parent" individuals to create offspring, aiming to improve solutions within the neighborhood.

Step 4. Update the population.

Eliminate individuals with poor performance based on the objective function.

Add new individuals generated in Step 3 if their performance is better.

Step 5. Repeat Steps 2, 3, and 4 for a specified number of iterations or until a termination criterion is met, corresponding to a sufficiently small objective function value.

The termination criteria may include reaching a maximum number of iterations, a convergence threshold for objective function values, or a predefined time limit.

Step 6. Select the individual with the best performance from the final population: The parameter set of this individual represents the optimal result for the Elman network using the BCMO algorithm.

Figure 3 illustrates the Elman network parameter optimization process using the BCMO.

5 Numerical results

This section presents an in-depth analysis of the proposed method's effectiveness in various earthquake scenarios. The testing structure platform is established on a three-story building with the detailed configuration in Table 2 as follows [67].

To be suitable for the conditions in reality, the maximum force of the active device, $u_{\max}$, is limited. In this paper, the value of $u_{\max}$ is set to 700 N. Moreover, the input variables of the proposed ENN model are evaluated into two different types: the full-state type and the 2-state type. To be more specific, the full-state type picks up six values, including the displacements and the velocities of all three floors $(x_1, x_2, x_3, \dot{x}_1, \dot{x}_2, \dot{x}_3)$. The 2-state type only chooses two values, including the displacement (x_1) and the velocity $(\dot{x}_1)$ of the first floor.

In the case of using the objective functions J_{D} and J_{A}, the notations for the full-state type and the 2-state type are presented in Table 3. As shown in Table 3, we developed four vibration controllers in total: the fNe_D controller, the fNe_A controller, the 2Ne_D controller, and the 2Ne_A controller.

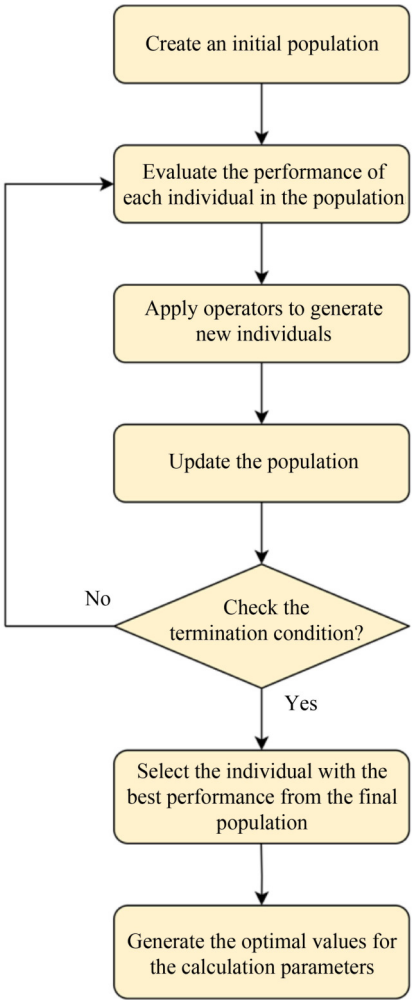

Fig. 3 The flowchart of the BCMO algorithm.

Table 2 The parameters of the three-story building

Parameter	Symbol	Value
Mass of the jth floor	$m_j, j = 1,2,3$	1000 (kg)
Damping coefficient of the jth floor	$c_j, j = 1,2,3$	1.407 (kN·s)/m
Stiffness coefficient of the jth floor	$k_j, j = 1,2,3$	980 (kN/m)

Table 3 The notations for the full-state type and the 2-state type

Type	Input values	Objective function	Notation
full-state	$x_1, x_2, x_3, \dot{x}_1, \dot{x}_2, \dot{x}_3$	$J_{\mathrm{D}} \rightarrow \min$	fNe_D
		$J_{\mathrm{A}} \rightarrow \min$	fNe_A
2-state	$x_1, \dot{x}_1$	$J_{\mathrm{D}} \rightarrow \min$	2Ne_D
		$J_{\mathrm{A}} \rightarrow \min$	2Ne_A

In this research, the data from the El Centro earthquake is selected as the environment excitation for finding the above-optimized parameters. After using the BCMO algorithm, the optimization values of the ENN core parameters are indicated in Table 4.

Table 4 The optimization values of the ENN core parameters

Controller	$w^{h,i}$	$w^{o,h}$	$w^{h,c}$	η	y	m
fNe_D	0.693	−0.337	0.337	1.406	1818.6	4
fNe_A	−0.161	0.752	0.426	2.468	2579.2	3
2Ne_D	−0.295	0.203	0.900	3.577	4761.5	2
2Ne_A	−0.965	−0.093	0.580	4.312	4894.9	2

Under the circumstance of the El Centro earthquake, the proposed ENN model is implemented and generates the vibration control results, as indicated in Fig. 4 and Table 5. To evaluate the efficiency of the optimization process, these results are also compared to those of other controllers, such as the LQR, the modified bang–bang controller (MBBC), the saturated sliding mode controller (SSMC), the robust saturation controller (RSC), the robust controller (RC) [67,72].

As shown in Fig. 4, it is noticeable that among all testing controllers, the fNE_A controller reached the lowest peak values of RD and AA on the highest floor. The 2Ne_A controller is the second-ranking for vibration reduction in the building structure. The results in Table 5 strongly confirm this conclusion. Specifically, Table 5 shows the value of each objective function and the controller's mean value. The fNe_A controller consistently delivers the best results compared to the rest of the controllers.

After optimizing the parameters of the proposed controllers by using the EI Centro earthquake data, their efficiency is also tested with other earthquakes to be more adaptive to reality. The limitation of control force is set up to 700 N. Figure 5 indicates the displacement results of the three-floor structure under earthquake excitations, including Kern County (1952), Tabas (1978), Northridge (1994), Kobe (1995), Duzce (1999), and Kocaeli (1999). To be more specific, the displacement graphs of the building under the influence of the controllers are shown in different colors, as follows: the gray curve denotes the case of without controlling; the red curve denotes the 2Ne_D controller; the blue curve is the 2Ne_A controller; the dash red curve is the fNe_D controller; and the dash blue curve is the fNe_A controller. It could be seen that, under the Kern County earthquake, the RD peak of the fNe_D controller is the smallest, followed by the RD peak of the 2Ne_A at the 2nd position. Meanwhile, in the Duzce earthquake, the 2Ne_A controller, the fNe_D controller, and the fNe_A controller generated almost the same RD peak values on the third floor. With the rest of the four earthquakes, the 2Ne_A controller maintains the lowest value of the displacement. These above findings show that the 2Ne_A controller is consistently the most effective in reducing structural displacement across a broad range of earthquakes. In other words, in the cases of Tabas, Northridge, Kobe, and Kocaeli earthquakes, the 2Ne_A controller could be chosen as a robust solution for earthquake protection. However, during the Kern County earthquake, the operation of the fNe_D controller outperforms the others. Additionally, there is an interesting point with the Duzce earthquake where multiple controllers (2Ne_A, fNe_D, fNe_A) offer nearly identical performance. This suggests that the natural characteristics of the earthquake may play a significant role in evaluating the controller's effectiveness.

Figure 6 depicts the building's acceleration graphs

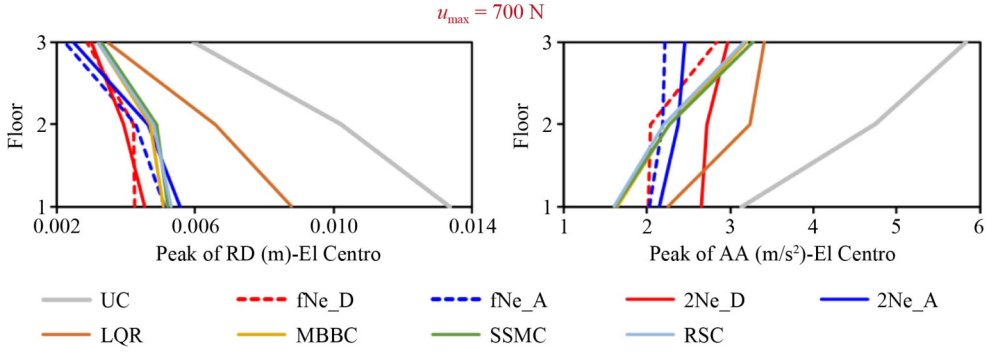

Fig. 4 The vibration response of the building structure under El Centro earthquake.

Table 5 The optimization values of the ENN core parameters

El Centro	fNe_D	fNe_A	2Ne_D	2Ne_A	LQR	MBBC	SSMC	RSC	RC
J_D	0.317	0.382	0.340	0.416	0.658	0.381	0.389	0.396	0.410
J_A	0.487	0.381	0.508	0.420	0.585	0.549	0.561	0.544	0.530
Mean	0.402	0.382	0.424	0.418	0.621	0.465	0.475	0.470	0.470

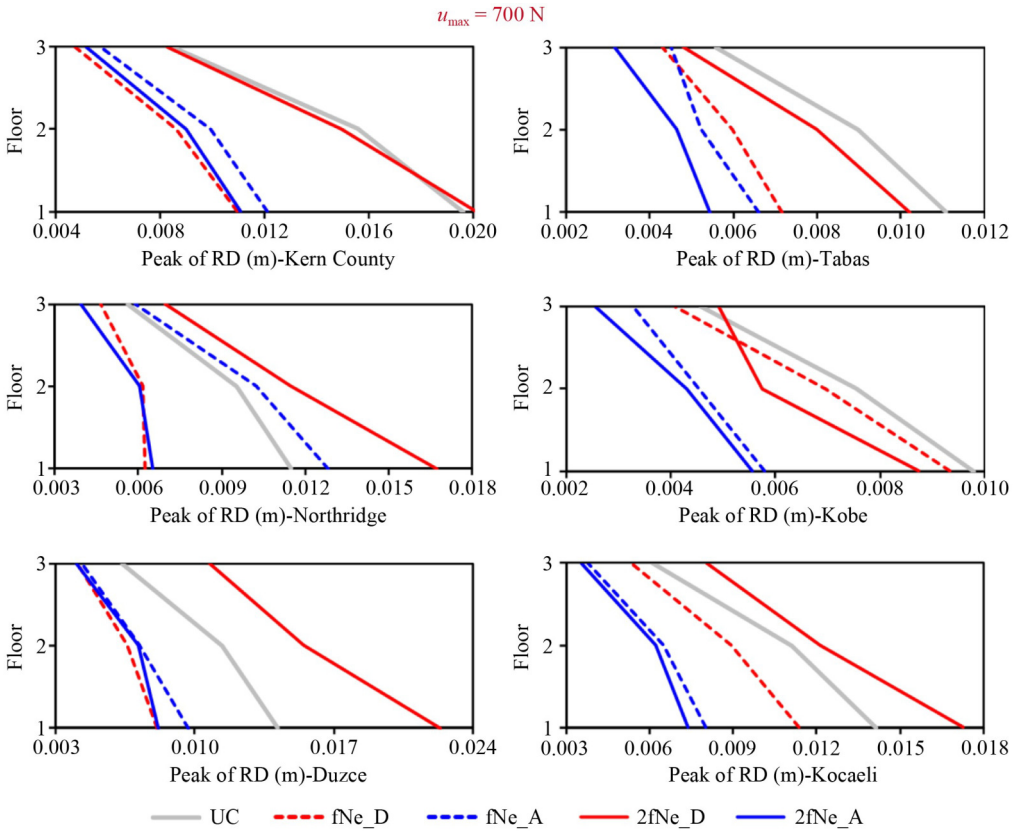

Fig. 5 The RD of the building structure under earthquakes.

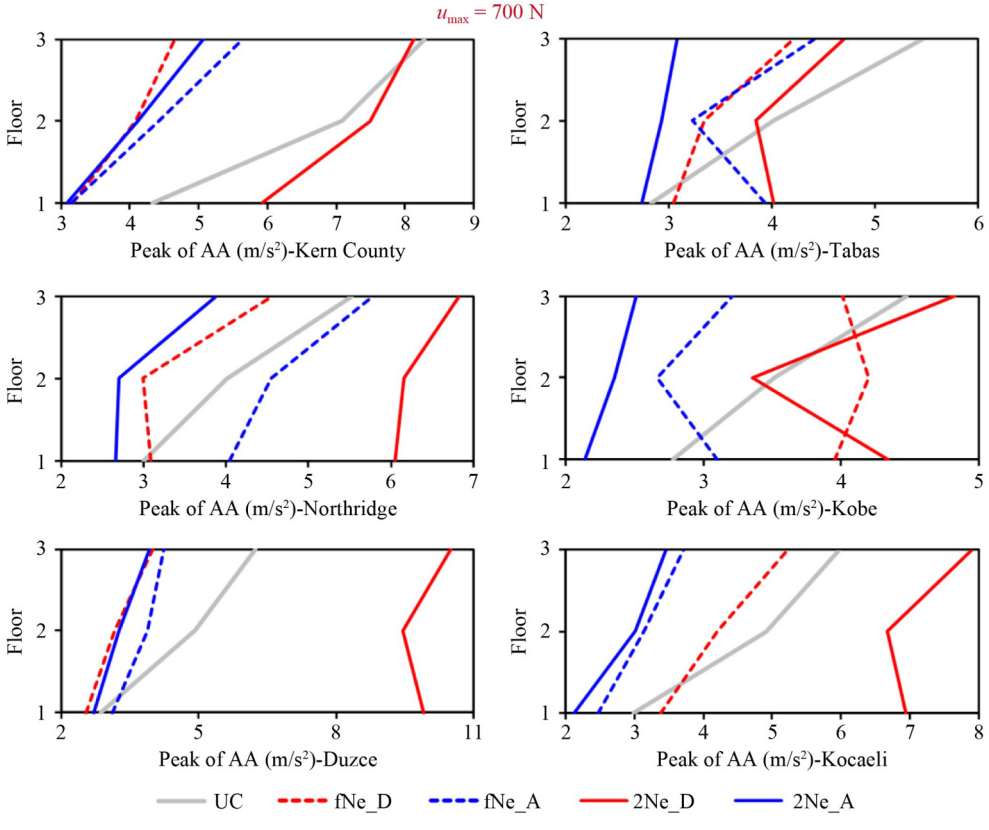

Fig. 6 The AA of the building structure under earthquakes.

under the impact of the mentioned controllers. To be more detailed, in the Tabas, Northridge, and Kobe earthquakes, the measured acceleration by using the 2Ne_A controller always reached smaller values compared to the others. Among four out of six earthquakes, the 2Ne_A controller minimizes acceleration on all floors, proving its robustness and reliability. However, during the Duzce earthquake and the Kern County earthquake, the first position belongs to the fNe_D controller, and the 2Ne_A controller is in the second position. This has again strengthened our conviction that certain earthquake scenarios may require different control methods to achieve optimal vibration reduction. The analysis underscores the importance of selecting the appropriate controller to reduce the responses of structures.

It is obvious that among the four considered controllers (the fNe_D controller, the fNe_A controller, the 2Ne_A controller, and the 2Ne_D controller), the results of choosing the best controller for vibration reduction could vary for each earthquake. Hence, this research applies more criteria to evaluate the performance of the proposed controllers. The criteria are the objective function J_D, the objective function J_A, and the mean values J_D and J_A. Table 6 presents the criterion findings for all the designed controllers across the seven earthquake tests.

As depicted in Table 6, the 2Ne_A controller has the smallest mean value of the objective functions, at about 0.556. This demonstrates that the 2Ne_A controller can be the most suitable for protecting the structure from earthquakes. Figure 7 shows the time responses of the RD on the first floor, the AA on the third floor, and the control force for the El Centro and Tabas earthquakes by using 2Ne_D and 2Ne_A, respectively.

Tables 7 and 8 show the reduction in building vibrations when applying the 2Ne_A controller to different earthquakes. The results show that the proposed controller is effective for the earthquakes that were investigated.

Table 6 The results of the objective functions for each earthquake

Earthquake	Criterion	fNe_D	fNe_A	2Ne_D	2Ne_A
El Centro	J_D	0.317	0.382	0.340	0.416
	J_A	0.487	0.381	0.508	0.420
	mean	0.402	0.381	0.424	0.418
Kern County	J_D	0.560	0.617	1.024	0.566
	J_A	0.562	0.682	0.983	0.613
	mean	0.561	0.649	1.004	0.589
Tabas	J_D	0.646	0.598	0.923	0.492
	J_A	0.771	0.808	0.859	0.565
	mean	0.708	0.703	0.891	0.528
Northridge	J_D	0.545	1.115	1.458	0.567
	J_A	0.823	1.043	1.232	0.701
	mean	0.684	1.079	1.345	0.634
Kobe	J_D	0.951	0.590	0.891	0.566
	J_A	0.896	0.718	1.080	0.561
	mean	0.923	0.654	0.986	0.564
Duzce	J_D	0.571	0.682	1.576	0.578
	J_A	0.642	0.679	1.684	0.632
	mean	0.606	0.680	1.630	0.605
Kocaeli	J_D	0.804	0.567	1.223	0.524
	J_A	0.874	0.622	1.324	0.580
	mean	0.839	0.594	1.273	0.552
Mean (all earthquakes)		0.675	0.677	1.079	0.556

In reality, many factors, such as mechanical wear, high temperatures, environmental conditions, and so on, could affect the active device quality after a long period of use. This could lead to a decline in the overall control force's

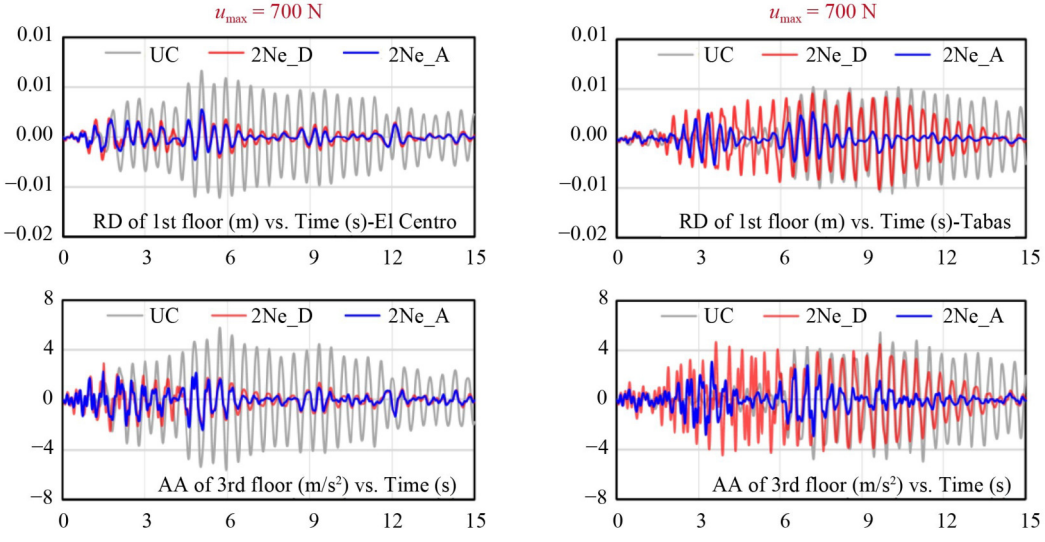

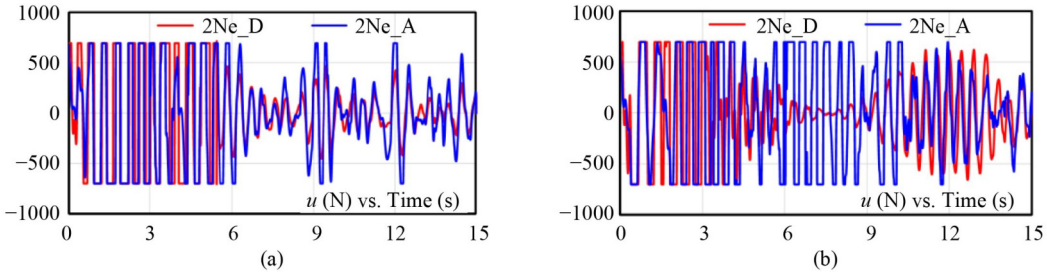

Fig. 7 The vibration response of the building structure: (a) El Centro earthquake; (b) Tabas earthquake.

Table 7 The maximum displacement on the 1st floor in the case of u_{max} = 700 N

Case	El Centro earthquake	Kern County earthquake	Tabas earthquake	Northridge earthquake	Kobe earthquake	Duzce earthquake	Kocaeli earthquake
Uncontrolled	0.0134	0.0196	0.0111	0.0115	0.0098	0.0142	0.0141
2Ne_A controller	0.0056	0.0111	0.0054	0.0065	0.0055	0.0082	0.0074
Reduction	58.21%	43.37%	51.35%	43.48%	43.88%	42.25%	47.52%

Table 8 The acceleration on the 3rd floor in the case of u_{max} = 700 N

Case	El Centro earthquake	Kern County earthquake	Tabas earthquake	Northridge earthquake	Kobe earthquake	Duzce earthquake	Kocaeli earthquake
Uncontrolled	5.8320	8.2784	5.4637	5.5306	4.4732	6.2400	5.9762
2Ne_A controller	2.4516	5.0717	3.0851	3.8746	2.5115	3.9427	3.4633
Reduction	57.96%	38.74%	43.53%	29.94%	43.85%	36.82%	42.05%

limitations. The evaluation stage for the impact of control force loss is an important issue that requires attention to ensure the proposed system's stability and efficiency during the operation process. In this research, the default value of the maximum control force is set to 700 N. Thus, we consider and assess the effectiveness of the suggested system by reducing this parameter to 90% and 80% of the standard value, which is 630 and 560 N, respectively. This testing aims to ensure that the proposed system can always work in optimal status and modify the controlling mode to be suitable for the change in the control force limitation. Tables 9 and 10 show the results of the mentioned case studies.

Table 9 indicates that the mean value of the fNe_A controller is the lowest, at about 0.652. This leads to the fact that the fNe_A shows the best performance among all earthquakes. Moreover, even when we decrease the maximum control force to 80% of the default value, fNE_A still maintains the smallest mean value. This same identification in Table 10 strengthened our conviction that the fNe_A controller is more suitable compared to the 2Ne_A controller.

Figure 8 illustrates the RD peak value and the AA peak value of all the mentioned controllers in the case of the El Centro earthquake, with the controller force being 560 N. Figures 9 and 10 display these parameters for six additional earthquakes.

Based on the above result, it is evident that if the

Table 9 The results of the objective functions for each earthquake (u_{max} = 630 N)

Earthquake	Criterion	fNe_D	fNe_A	2Ne_D	2Ne_A
El Centro	J_D	0.422	0.446	0.463	0.444
	J_A	0.548	0.498	0.484	0.511
	mean	0.485	0.472	0.473	0.478
Kern County	J_D	0.604	0.679	1.066	0.705
	J_A	0.605	0.725	1.168	0.805
	mean	0.605	0.702	1.117	0.755
Tabas	J_D	1.036	0.577	1.177	0.508
	J_A	1.012	0.673	1.005	0.546
	mean	1.024	0.625	1.091	0.527
Northridge	J_D	0.588	0.808	1.061	0.617
	J_A	0.841	0.805	1.016	0.712
	mean	0.715	0.806	1.039	0.664
Kobe	J_D	0.931	0.612	0.771	0.670
	J_A	0.870	0.705	0.789	0.709
	mean	0.901	0.659	0.780	0.690
Duzce	J_D	0.893	0.698	0.786	0.608
	J_A	0.924	0.679	0.883	0.655
	mean	0.908	0.688	0.834	0.631
Kocaeli	J_D	0.806	0.590	1.422	0.819
	J_A	0.858	0.631	1.401	0.912
	mean	0.832	0.611	1.411	0.866
Mean (all earthquakes)		0.781	0.652	0.964	0.659

Table 10 The results of the objective functions for each earthquake (u_{max} = 560 N)

Earthquake	Criterion	fNe_D	fNe_A	2Ne_D	2Ne_A
El Centro	J_D	0.454	0.506	0.538	0.650
	J_A	0.569	0.549	0.512	0.791
	mean	0.512	0.528	0.525	0.720
Kern County	J_D	0.648	0.740	1.069	0.775
	J_A	0.648	0.796	1.286	0.852
	mean	0.648	0.768	1.177	0.814
Tabas	J_D	0.601	0.614	1.365	0.550
	J_A	0.695	0.638	1.214	0.576
	mean	0.648	0.626	1.290	0.563
Northridge	J_D	0.620	0.750	1.114	0.648
	J_A	0.856	0.851	0.973	0.740
	mean	0.738	0.800	1.044	0.694
Kobe	J_D	0.947	0.630	0.933	0.636
	J_A	0.845	0.640	0.995	0.636
	mean	0.896	0.635	0.964	0.636
Duzce	J_D	0.629	0.707	1.085	0.730
	J_A	0.681	0.716	1.050	0.747
	mean	0.655	0.712	1.067	0.738
Kocaeli	J_D	0.808	0.624	0.916	0.796
	J_A	0.834	0.647	0.968	0.811
	mean	0.821	0.635	0.942	0.804
Mean (all earthquakes)		0.703	0.672	1.001	0.710

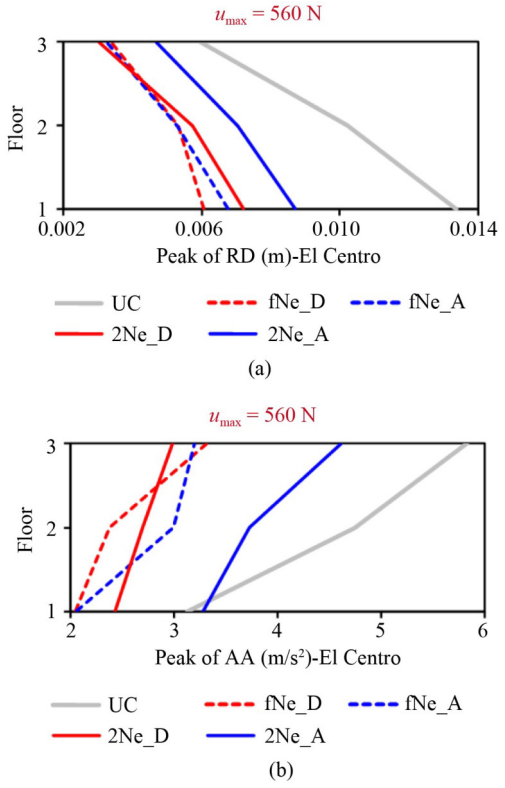

Fig. 8 The peak of RD and AA of the building structure under El Centro earthquake: (a) the peak of RD; (b) the peak of AA.

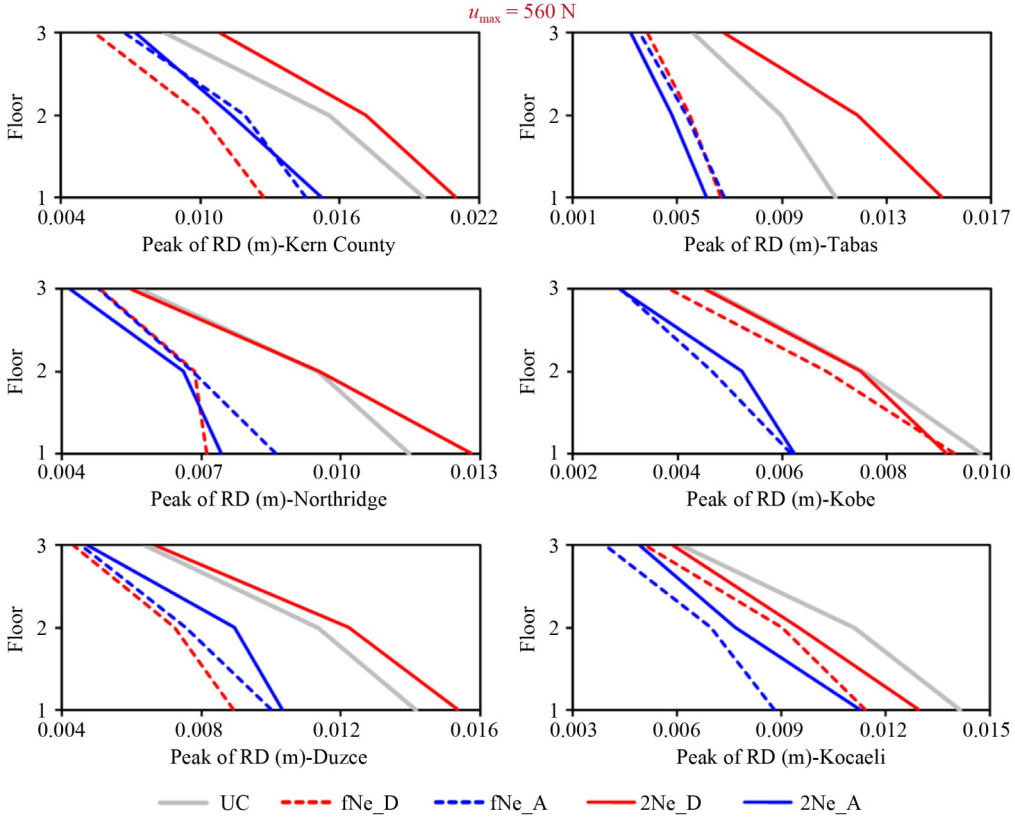

Fig. 9 The peak of RD of the building structure under other earthquakes.

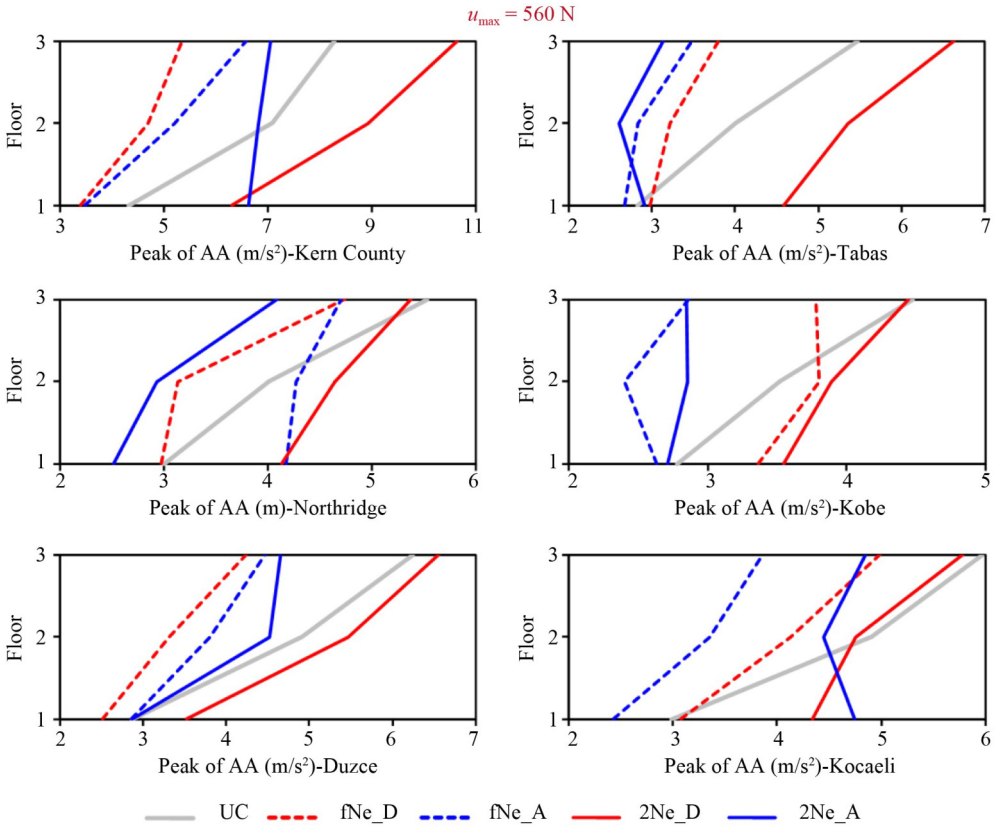

Fig. 10 The peak of AA of the building structure under other earthquakes.

quality deterioration phenomenon occurs on the active device and the control force limitation is reduced to 80%–90% of the ordinary value, and the controlling mode needs to be switched to the fNe_A controller instead of the 2Ne_A controller.

6 Conclusions

The research proposed an updated Elman network with an adjustment coefficient in the output layer to improve the controller's performance for earthquake-induced structural vibrations. The suggested network's parameters were optimized using the BCMO method and El Centro seismic data. These optimal parameters are then used to evaluate the controller's performance in decreasing building vibrations caused by further earthquakes. The verification demonstrated that the controller has a high level of generality and can be used for a wide variety of earthquakes. Furthermore, even if the active damping device loses its maximum force value, the suggested controller remains effective, particularly when employing the 2Ne_A controller. This paper's findings give academics and engineers a fresh viewpoint on the use of AI to reduce vibrations in structural works. This is not only a foundation for theoretical advancement, but it also opens up practical opportunities for using AI in building and seismic safety for structures.

Acknowledgements This research was funded by Hanoi University of Science and Technology, Vietnam (No. T2023-PC-013).

Competing interests The authors declare that they have no competing interests.

References

1. Firouzi N, Dohnal F. Dynamic stability of the Mindlin-Reissner plate using a time-modulated axial force. Mechanics Based Design of Structures and Machines, 2024: 1–18
2. Tran N A, Bui H L, Cao Q H. U-shaped and V-shaped tuned liquid column dampers in vibration reduction of earthquake-induced buildings: A comparative study. Structures, 2024, 65: 106669
3. Tran N A, Bui V B, Bui H L. Optimization of multi-TMD using BCMO algorithm for building models subjected to earthquake. In: Proceedings of International Conference on Engineering Research and Applications. Nguyen: Springer Nature Switzerland, 2023, 293–298
4. Hu Y, Hua T, Chen M Z, Shi S, Sun Y. Instability analysis for semi-active control systems with semi-active inerters. Nonlinear Dynamics, 2021, 105(1): 99–112
5. Lu Z, Zhou M, Zhang J, Huang Z, Masri S F. A semi-active impact damper for multi-modal vibration control under earthquake excitations. Mechanical Systems and Signal Processing, 2024, 210: 111182

6. Bui H L, Nguyen T D, Le V D. Optimal design of hedge-algebras-based controller for active suspension systems with parameter uncertainty. In: Proceedings of International Conference on Advances in Information and Communication Technology. Nguyen: Springer, 2023, 163–170
7. Mac T T, Nguyen T D, Bui H L, Tran N A. Optimal design of hedge-algebras-based controller for vibration control of vehicle suspension systems. Journal of Systems and Control Engineering, 2024, 238(4): 755–776
8. Hai-Le Bui I. Optimal design using BCMO algorithm of fuzzy controllers for active suspension. In: Proceedings of the International Conference on Engineering Research and Applications, ICERA 2023. Nguyen: Springer, 2024, 271
9. Bui H L, Tran N A, Cao H Q. Active control based on hedge-algebras theory of seismic-excited buildings with upgraded tuned liquid column damper. Journal of Engineering Mechanics, 2023, 149(1): 04022091
10. Cao H Q, Tran N A, Bui H L. Hedge-Algebras-based hybrid control of earthquake-induced buildings using upgraded tuned liquid column dampers. Soil Dynamics and Earthquake Engineering, 2024, 182: 108728
11. Friis T, Katsanos E I, Saberi M, Koss H H H. Two-level friction damping and its application for passive multi-functional vibration control of high-rise buildings. Engineering Structures, 2021, 239: 112310
12. Cao H Q, Tran N A, Nguyen X T. Tuned two-mass dampers for vibration control of offshore platforms. Engineering Research Express, 2024, 6(3): 035511
13. Baduidana M, Kenfack-Jiotsa A. Minimization of the primary structure response under random excitation using high-performance passive tuned mass damper ineter control configurations. Journal of Vibration Engineering & Technologies, 2024, 12: 37–47
14. Cheng Y, Ji X. Robustness of a tuned viscous mass damper (TVMD) controlled system. Advances in Structural Engineering, 2022, 25(16): 3349–3367
15. Shirai K, Sano T, Suzui Y. Energy response of a passive variable friction damper and numerical simulation on the control effects for high-rise buildings. Structural Control and Health Monitoring, 2022, 29(12): e3124
16. Chowdhury S, Banerjee A, Adhikari S. Optimal design of inertial amplifier base isolators for dynamic response control of multi-storey buildings. International Journal of Structural Stability and Dynamics, 2023, 23(5): 2350047
17. Addala M B, Bhalla S, Madan A. Controlling dynamic response of structures using hybrid passive energy dissipation device. Journal of Earthquake Engineering, 2022, 26(6): 3209–3227
18. Li L y, Zhang T. Analytical analysis for the design of nonlinear tuned mass damper. Journal of Vibration and Control, 2020, 26(9–10): 646–658
19. Sharma K V, Parmar V, Gautam L, Choudhary S, Gohil J. Modelling efficiency of fluid viscous dampers positioning for increasing tall buildings' Resilience to earthquakes induced structural vibrations. Soil Dynamics and Earthquake Engineering, 2023, 173: 108108
20. Barzegar V, Laflamme S, Downey A, Li M, Hu C. Numerical evaluation of a novel passive variable friction damper for vibration mitigation. Engineering Structures, 2020, 220: 110920
21. Li H, Yang H T, Kwon I Y, Ly F S. Bio-inspired passive base isolator with tuned mass damper inerter for structural control. Smart Materials and Structures, 2019, 28(10): 105008
22. Zhou Y, Aguaguiña M, Beskos D E, Gong S. A displacement-based seismic design method for building structures with nonlinear viscoelastic dampers. Bulletin of Earthquake Engineering, 2021, 19(11): 4535–4585
23. Hagedorn P, Spelsberg-Korspeter G. Active and Passive Vibration Control of Structures. New York, NY: Springer, 2014
24. Zelleke D H, Matsagar V A. Semi-active algorithm for energy-based predictive structural control using tuned mass dampers. Computer-Aided Civil and Infrastructure Engineering, 2019, 34(11): 1010–1025
25. Altay O, Klinkel S. CANFIS-based semi-active vibration control of stochastically excited high-rise civil engineering structures with nonlinearities and uncertainties. Proceedings in Applied Mathematics and Mechanics, 2019, 19(1): e201900132
26. Ghorbanzadeh M, Sensoy S, Uygar E. Seismic performance assessment of semi active tuned mass damper in an MRF steel building including nonlinear soil–pile–structure interaction. Arabian Journal for Science and Engineering, 2023, 48(4): 4675–4693
27. Chha H, Peng Y. Adaptive semiactive control of structure with magnetorheological dampers using wavelet packet transform. Advances in Structural Engineering, 2024, 27(9): 13694332241254606
28. Menezes Morato M, Pham T P, Sename O, Dugard L. Development of a simple ER damper model for fault-tolerant control design. Journal of the Brazilian Society of Mechanical Sciences and Engineering, 2020, 42(10): 1–22
29. Bhowmik K, Debnath N. Semi-active vibration control of soft-storey building with magnetorheological damper under seismic Excitation. Journal of Vibration Engineering & Technologies, 2024, 12(4): 6943–6961
30. Tang X, Ning D, Du H, Li W, Wen W. Takagi-sugeno fuzzy model-based semi-active control for the seat suspension with an electrorheological damper. IEEE Access, 2020, 8: 98027–98037
31. Magdaleno A, Pereira E, Reynolds P, Lorenzana A. A common framework for tuned and active mass dampers: Application to a two-Storey building model. Experimental Techniques, 2021, 45(5): 661–671
32. Ito T, Tagami M, Tagawa Y. Active vibration control for high-rise buildings using displacement measurements by image processing. Structural Control and Health Monitoring, 2022, 29(12): e3136
33. Zhang H, Shan J, Lu X. Field testing and performance evaluation of AMD-controlled high-rise building structures with real-world validation. Journal of Building Engineering, 2023, 80: 108109
34. Zhou K, Li Q S. Vibration mitigation performance of active tuned mass damper in a super high-rise building during multiple tropical storms. Engineering Structures, 2022, 269: 114840
35. Ershadbakhsh A M, Ghorbani-Tanha A K, Fallahi R. A novel active tendon pendulum tuned mass damper and its application in transient vibration control. Structures, 2023, 47: 2273–2280
36. Bui H L. An approach for optimizing the hedge-algebras-based

controller and application in structural vibration control. In: Proceedings of International Conference on Engineering Research and Applications. Cham: Springer, 2022, 157–165
37. Sharma A, Gautam R, Singh J. Deep learning for face mask detection: A survey. Multimedia Tools and Applications, 2023, 82(22): 34321–34361
38. Wang Y C, Chi O H, Saito H, Lu Y D. Conversational AI chatbots as counselors for hospitality employees. International Journal of Hospitality Management, 2024, 122: 103861
39. Bui H A, Nguyen A T, Nguyen T T. Develop a navigation approach for mobile robots based on the distributional deep reinforcement learning framework. In: Proceedings of 2024 IEEE 11th International Conference on Computational Cybernetics and Cyber-Medical Systems (ICCC). Hanoi: IEEE, 2024, 1–6
40. Anitescu C, Atroshchenko E, Alajlan N, Rabczuk T. Artificial neural network methods for the solution of second order boundary value problems. Computers, Materials & Continua, 2019, 59(1): 345–359
41. Samaniego E, Anitescu C, Goswami S, Nguyen-Thanh V M, Guo H, Hamdia K, Zhuang X, Rabczuk T. An energy approach to the solution of partial differential equations in computational mechanics via machine learning: Concepts, implementation and applications. Computer Methods in Applied Mechanics and Engineering, 2020, 362: 112790
42. Tariq S, Khalid U, Arfeto B E, Duong T Q, Shin H. Integrating sustainable big AI: Quantum anonymous semantic broadcast. IEEE Wireless Communications, 2024, 31(3): 86–99
43. Gupta S, Modgil S, Kumar A, Sivarajah U, Irani Z. Artificial intelligence and cloud-based collaborative platforms for managing disaster, extreme weather and emergency operations. International Journal of Production Economics, 2022, 254: 108642
44. Chen J, Cho Y K. CrackEmbed: Point feature embedding for crack segmentation from disaster site point clouds with anomaly detection. Advanced Engineering Informatics, 2022, 52: 101550
45. Chen Z, Wagner M, Das J, Doe R K, Cerveny R S. Data-driven approaches for tornado damage estimation with unpiloted aerial systems. Remote Sensing, 2021, 13(9): 1669
46. Chen J, Li Y, Zhang S. Fast prediction of urban flooding water depth based on CNN−LSTM. Water, 2023, 15(7): 1397
47. Li L, Wu W, Zhang W, Zhu Z, Li Z, Wang Y, Niu S. Storm surge level prediction based on improved NARX neural network. Journal of Computational Electronics, 2023, 22(2): 783–804
48. Kolivand P, Saberian P, Tanhapour M, Karimi F, Kalhori S R N, Javanmard Z, Heydari S, Talari S S H, Mousavi S M L, Alidadi M, et al. A systematic review of earthquake early warning (EEW) systems based on artificial intelligence. Earth Science Informatics, 2024, 17(2): 957–984
49. Jamil M, Khan M N, Rind S J, Awais Q, Uzair M. Neural network predictive control of vibrations in tall structure: An experimental controlled vision. Computers & Electrical Engineering, 2021, 89: 106940
50. Zizouni K, Fali L, Sadek Y, Bousserhane I K. Neural network control for earthquake structural vibration reduction using MRD. Frontiers of Structural and Civil Engineering, 2019, 13(5): 1171–1182
51. Goswami S, Anitescu C, Chakraborty S, Rabczuk T. Transfer learning enhanced physics informed neural network for phase-field modeling of fracture. Theoretical and Applied Fracture Mechanics, 2020, 106: 102447
52. Qiu Z, Wang T. Fuzzy neural network vibration control on a piezoelectric flexible hinged plate using stereo vision detection. Journal of Intelligent Material Systems and Structures, 2019, 30(4): 556–575
53. Paneiro G, Rafael M. Artificial neural network with a cross-validation approach to blast-induced ground vibration propagation modeling. Underground Space, 2021, 6(3): 281–289
54. Li S, He P, Nguang S K, Lin X. Barrier function-based adaptive neuro network sliding mode vibration control for flexible double-clamped beams with input saturation. IEEE Access, 2020, 8: 125887–125898
55. Yan X, Xu Z D, Shi Q X. Fuzzy neural network control algorithm for asymmetric building structure with active tuned mass damper. Journal of Vibration and Control, 2020, 26(21–22): 2037–2049
56. Brancati R, Di Massa G, Pagano S, Petrillo A, Santini S. A combined neural network and model predictive control approach for ball transfer unit—Magnetorheological elastomer-based vibration isolation of lightweight structures. Journal of Vibration and Control, 2020, 26(19–20): 1668–1682
57. Yucesan Y A, Viana F A, Manin L, Mahfoud J. Adjusting a torsional vibration damper model with physics-informed neural networks. Mechanical Systems and Signal Processing, 2021, 154: 107552
58. Xing X, Liu J. Modelling and neural adaptive vibration control for three-dimensional Timoshenko beam with output restrictions and external disturbances. International Journal of Systems Science, 2021, 52(9): 1850–1867
59. Zhang Y, Ma H, Xu J. Neural network-based fuzzy vibration controller for offshore platform with random time delay. Ocean Engineering, 2021, 225: 108733
60. Zhang H, Zhang R, He Q, Liu L. Variable universe fuzzy control of high-speed elevator horizontal vibration based on firefly algorithm and backpropagation fuzzy neural network. IEEE Access, 2021, 9: 57020–57032
61. Yu T, Mu Z, Johnson E A. Real-time neural network based semiactive model predictive control of structural vibrations. Computers & Structures, 2023, 275: 106899
62. Song H, Shan X, Zhang L, Wang G, Fan J. Research on identification and active vibration control of cantilever structure based on NARX neural network. Mechanical Systems and Signal Processing, 2022, 171: 108872
63. Qiu Z, Chen S. Vibration control of a translational coupled double flexible beam system using sliding mode neural network fuzzy control. Transactions of the Institute of Measurement and Control, 2022, 44(11): 2264–2288
64. Gheni E Z, Al-Khafaji H M, Alwan H M. A deep reinforcement learning framework to modify LQR for an active vibration control applied to 2D building models. Open Engineering, 2024, 14(1): 20220496
65. Zhang J, Xue Y. Intelligent control method research for high rise building vibration by integrating genetic algorithm and LSTM. IEEE Access, 2023, 12: 9810–9821
66. Bui V B, Mac T T, Bui H L. Design optimization considering the

stability constraint of the Hedge-algebras-based controller for building structures subjected to seismic excitations. Journal of Systems and Control Engineering, 2023, 237(10): 1822–1837

67. Du H, Zhang N, Naghdy F. Actuator saturation control of uncertain structures with input time delay. Journal of Sound and Vibration, 2011, 330(18–19): 4399–4412
68. Le-Duc T, Nguyen Q H, Nguyen-Xuan H. Balancing composite motion optimization. Information Sciences, 2020, 520: 250–270
69. Nguyen T D, Bui H L. General optimization procedure of the Hedge-algebras controller for controlling dynamic systems. Artificial Intelligence Review, 2023, 56(3): 2749–2784
70. Nguyen S T, Mac T T, Bui H L. Motion control of a mobile robot using the hedge-algebras-based controller. Journal of Robotics, 2023, 2023: 6613293
71. Nguyen T D, Nguyen S T, Mac T T, Bui H L. Trajectory tracking of mobile robots using hedge-agebras-based controllers. Intelligent Service Robotics, 2024, 17(4): 1–22
72. Lim C, Park Y, Moon S. Robust saturation controller for linear time-invariant system with structured real parameter uncertainties. Journal of Sound and Vibration, 2006, 294(1–2): 1–14